Research Article | Vol. 25, No. 14 | 10 Jul 2017 | OPTICS EXPRESS 15927
Optics EXPRESS

Boosting magnetic field enhancement with radiative couplings of magnetic modes in dielectric nanostructures

ZHONG-JIAN YANG,[1,*] QIAN ZHAO,[1] AND JUN HE[1,2]

[1]*Hunan Key Laboratory of Super Microstructure and Ultrafast Process, School of Physics and Electronics, Central South University, Changsha, Hunan 410083, China*
[2]*junhe@csu.edu.cn*
[*]*zjyang@csu.edu.cn*

Abstract: Dielectric nanostructures can readily support considerable magnetic field enhancements that offer great potential applications in field enhanced spectroscopies. However, the magnetic fields of dielectric structures are usually distributed within the entire volume, which brings challenge to the further increment of the magnetic field enhancement. Here, we theoretically demonstrate that the magnetic field enhancement in dielectric nanostructures can be boosted through the radiative couplings of magnetic modes. Our concentric structure consists of a hollow disk and a ring. The disk has a magnetic dipole mode. The ring has two magnetic dipole modes that are out of phase. Strong radiative interactions between the modes on the disk and the ring can occur, which result in a net constructive coupling effect. For a lossless material with $n = 3.3$, a sharp peak can be obtained on the scattering spectrum of the coupled system due to the radiative interactions. The corresponding resonant magnetic field enhancement at the disk center reaches 96 times. This enhancement is about 7 times higher than that of an individual disk. The structure with a lossy material Si is also considered, where radiative couplings and boosted magnetic field can also be obtained. Our research reveals the strong radiative mode couplings in dielectric structures and is important for furthering our understanding on the light-matter interactions at the nanoscale.

OCIS codes: (350.4238) Nanophotonics and photonic crystals; (310.6628) Subwavelength structures, nanostructures.

References and links

1. A. I. Kuznetsov, A. E. Miroshnichenko, M. L. Brongersma, Y. S. Kivshar, and B. Luk'yanchuk, "Optically resonant dielectric nanostructures," Science **354**(6314), aag2472 (2016).
2. M. Decker and I. Staude, "Resonant dielectric nanostructures: a low-loss platform for functional nanophotonics," J. Opt. **18**(10), 103001 (2016).
3. M. Khorasaninejad, W. T. Chen, R. C. Devlin, J. Oh, A. Y. Zhu, and F. Capasso, "Metalenses at visible wavelengths: Diffraction-limited focusing and subwavelength resolution imaging," Science **352**(6290), 1190–1194 (2016).
4. P. Genevet, F. Capasso, F. Aieta, M. Khorasaninejad, and R. Devlin, "Recent advances in planar optics: from plasmonic to dielectric metasurfaces," Optica **4**(1), 139–152 (2017).
5. D. Lin, P. Fan, E. Hasman, and M. L. Brongersma, "Dielectric gradient metasurface optical elements," Science **345**(6194), 298–302 (2014).
6. Z. Zhou, J. Li, R. Su, B. Yao, H. Fang, K. Li, L. Zhou, J. Liu, D. Stellinga, C. P. Reardon, T. F. Krauss, and X. Wang, "Efficient Silicon Metasurfaces for Visible Light," ACS Photonics **4**(3), 544–551 (2017).
7. A. Arbabi, Y. Horie, M. Bagheri, and A. Faraon, "Dielectric metasurfaces for complete control of phase and polarization with subwavelength spatial resolution and high transmission," Nat. Nanotechnol. **10**(11), 937–943 (2015).
8. S. Jahani and Z. Jacob, "All-dielectric metamaterials," Nat. Nanotechnol. **11**(1), 23–36 (2016).
9. W. Fan, B. Yan, Z. Wang, and L. Wu, "Three-dimensional all-dielectric metamaterial solid immersion lens for subwavelength imaging at visible frequencies," Sci. Adv. **2**(8), e1600901 (2016).
10. P. Moitra, Y. Yang, Z. Anderson, I. I. Kravchenko, D. P. Briggs, and J. Valentine, "Realization of an all-dielectric zero-index optical metamaterial," Nat. Photonics **7**(10), 791–795 (2013).
11. M. L. Brongersma, Y. Cui, and S. Fan, "Light management for photovoltaics using high-index nanostructures," Nat. Mater. **13**(5), 451–460 (2014).

#295208 https://doi.org/10.1364/OE.25.015927
Journal © 2017 Received 3 May 2017; revised 20 Jun 2017; accepted 23 Jun 2017; published 27 Jun 2017

Optics EXPRESS

12. Y. Cui, D. van Dam, S. A. Mann, N. J. van Hoof, P. J. van Veldhoven, E. C. Garnett, E. P. Bakkers, and J. E. Haverkort, "Boosting solar cell photovoltage via nanophotonic engineering," Nano Lett. **16**(10), 6467–6471 (2016).
13. M. Caldarola, P. Albella, E. Cortés, M. Rahmani, T. Roschuk, G. Grinblat, R. F. Oulton, A. V. Bragas, and S. A. Maier, "Non-plasmonic nanoantennas for surface enhanced spectroscopies with ultra-low heat conversion," Nat. Commun. **6**, 7915 (2015).
14. T. Shibanuma, P. Albella, and S. A. Maier, "Unidirectional light scattering with high efficiency at optical frequencies based on low-loss dielectric nanoantennas," Nanoscale **8**(29), 14184–14192 (2016).
15. X. Zambrana-Puyalto and N. Bonod, "Tailoring the chirality of light emission with spherical Si-based antennas," Nanoscale **8**(19), 10441–10452 (2016).
16. A. E. Krasnok, A. E. Miroshnichenko, P. A. Belov, and Y. S. Kivshar, "All-dielectric optical nanoantennas," Opt. Express **20**(18), 20599–20604 (2012).
17. M. K. Schmidt, R. Esteban, J. J. Sáenz, I. Suárez-Lacalle, S. Mackowski, and J. Aizpurua, "Dielectric antennas--a suitable platform for controlling magnetic dipolar emission," Opt. Express **20**(13), 13636–13650 (2012).
18. D. Lin, A. L. Holsteen, E. Maguid, G. Wetzstein, P. G. Kik, E. Hasman, and M. L. Brongersma, "Photonic Multitasking Interleaved Si Nanoantenna Phased Array," Nano Lett. **16**(12), 7671–7676 (2016).
19. D. Smirnova and Y. S. Kivshar, "Multipolar nonlinear nanophotonics," Optica **3**(11), 1241–1255 (2016).
20. M. R. Shcherbakov, D. N. Neshev, B. Hopkins, A. S. Shorokhov, I. Staude, E. V. Melik-Gaykazyan, M. Decker, A. A. Ezhov, A. E. Miroshnichenko, I. Brener, A. A. Fedyanin, and Y. S. Kivshar, "Enhanced third-harmonic generation in silicon nanoparticles driven by magnetic response," Nano Lett. **14**(11), 6488–6492 (2014).
21. P. R. Wiecha, A. Arbouet, C. Girard, T. Baron, and V. Paillard, "Origin of second-harmonic generation from individual silicon nanowires," Phys. Rev. B **93**(12), 125421 (2016).
22. S. Zhang, R. Jiang, Y. M. Xie, Q. Ruan, B. Yang, J. Wang, and H. Q. Lin, "Colloidal Moderate-Refractive-Index Cu_2O Nanospheres as Visible-Region Nanoantennas with Electromagnetic Resonance and Directional Light-Scattering Properties," Adv. Mater. **27**(45), 7432–7439 (2015).
23. A. I. Kuznetsov, A. E. Miroshnichenko, Y. H. Fu, J. Zhang, and B. Luk'yanchuk, "Magnetic light," Sci. Rep. **2**, 492 (2012).
24. Y. H. Fu, A. I. Kuznetsov, A. E. Miroshnichenko, Y. F. Yu, and B. Luk'yanchuk, "Directional visible light scattering by silicon nanoparticles," Nat. Commun. **4**, 1527 (2013).
25. M. I. Tribelsky and A. E. Miroshnichenko, "Giant in-particle field concentration and Fano resonances at light scattering by high-refractive-index particles," Phys. Rev. A **93**(5), 053837 (2016).
26. A. B. Evlyukhin, S. M. Novikov, U. Zywietz, R. L. Eriksen, C. Reinhardt, S. I. Bozhevolnyi, and B. N. Chichkov, "Demonstration of magnetic dipole resonances of dielectric nanospheres in the visible region," Nano Lett. **12**(7), 3749–3755 (2012).
27. I. Staude, A. E. Miroshnichenko, M. Decker, N. T. Fofang, S. Liu, E. Gonzales, J. Dominguez, T. S. Luk, D. N. Neshev, I. Brener, and Y. Kivshar, "Tailoring directional scattering through magnetic and electric resonances in subwavelength silicon nanodisks," ACS Nano **7**(9), 7824–7832 (2013).
28. T. G. Habteyes, I. Staude, K. E. Chong, J. Dominguez, M. Decker, A. Miroshnichenko, Y. Kivshar, and I. Brener, "Near-field mapping of optical modes on all-dielectric silicon nanodisks," ACS Photonics **1**(9), 794–798 (2014).
29. W. Liu, J. Zhang, B. Lei, H. Hu, and A. E. Miroshnichenko, "Invisible nanowires with interfering electric and toroidal dipoles," Opt. Lett. **40**(10), 2293–2296 (2015).
30. A. E. Miroshnichenko, A. B. Evlyukhin, Y. F. Yu, R. M. Bakker, A. Chipouline, A. I. Kuznetsov, B. Luk'yanchuk, B. N. Chichkov, and Y. S. Kivshar, "Nonradiating anapole modes in dielectric nanoparticles," Nat. Commun. **6**, 8069 (2015).
31. P. Fan, Z. Yu, S. Fan, and M. L. Brongersma, "Optical Fano resonance of an individual semiconductor nanostructure," Nat. Mater. **13**(5), 471–475 (2014).
32. L. Huang, Y. Yu, and L. Cao, "General modal properties of optical resonances in subwavelength nonspherical dielectric structures," Nano Lett. **13**(8), 3559–3565 (2013).
33. H.-S. Ee, J.-H. Kang, M. L. Brongersma, and M.-K. Seo, "Shape-dependent light scattering properties of subwavelength silicon nanoblocks," Nano Lett. **15**(3), 1759–1765 (2015).
34. U. Zywietz, M. K. Schmidt, A. B. Evlyukhin, C. Reinhardt, J. Aizpurua, and B. N. Chichkov, "Electromagnetic resonances of silicon nanoparticle dimers in the visible," ACS Photonics **2**(7), 913–920 (2015).
35. J. van de Groep, T. Coenen, S. A. Mann, and A. Polman, "Direct imaging of hybridized eigenmodes in coupled silicon nanoparticles," Optica **3**(1), 93–99 (2016).
36. Y. Yang, I. I. Kravchenko, D. P. Briggs, and J. Valentine, "All-dielectric metasurface analogue of electromagnetically induced transparency," Nat. Commun. **5**, 5753 (2014).
37. C. Wu, N. Arju, G. Kelp, J. A. Fan, J. Dominguez, E. Gonzales, E. Tutuc, I. Brener, and G. Shvets, "Spectrally selective chiral silicon metasurfaces based on infrared Fano resonances," Nat. Commun. **5**, 3892 (2014).
38. J. Yan, P. Liu, Z. Lin, H. Wang, H. Chen, C. Wang, and G. Yang, "Directional Fano resonance in a silicon nanosphere dimer," ACS Nano **9**(3), 2968–2980 (2015).
39. B. Hopkins, D. S. Filonov, A. E. Miroshnichenko, F. Monticone, A. Alù, and Y. S. Kivshar, "Interplay of magnetic responses in all-dielectric oligomers to realize magnetic Fano resonances," ACS Photonics **2**(6), 724–729 (2015).

Optics EXPRESS

40. Z.-J. Yang, "Fano Interference of Electromagnetic Modes in Subwavelength Dielectric Nanocrosses," J. Phys. Chem. C **120**(38), 21843–21849 (2016).
41. P. Albella, M. A. Poyli, M. K. Schmidt, S. A. Maier, F. Moreno, J. J. Sáenz, and J. Aizpurua, "Low-loss electric and magnetic field-enhanced spectroscopy with subwavelength silicon dimers," J. Phys. Chem. C **117**(26), 13573–13584 (2013).
42. R. M. Bakker, D. Permyakov, Y. F. Yu, D. Markovich, R. Paniagua-Domínguez, L. Gonzaga, A. Samusev, Y. Kivshar, B. Luk'yanchuk, and A. I. Kuznetsov, "Magnetic and electric hotspots with silicon nanodimers," Nano Lett. **15**(3), 2137–2142 (2015).
43. A. Mirzaei and A. E. Miroshnichenko, "Electric and magnetic hotspots in dielectric nanowire dimers," Nanoscale **7**(14), 5963–5968 (2015).
44. T. Feng, Y. Xu, Z. Liang, and W. Zhang, "All-dielectric hollow nanodisk for tailoring magnetic dipole emission," Opt. Lett. **41**(21), 5011–5014 (2016).
45. M. Kasperczyk, S. Person, D. Ananias, L. D. Carlos, and L. Novotny, "Excitation of magnetic dipole transitions at optical frequencies," Phys. Rev. Lett. **114**(16), 163903 (2015).
46. C. M. Dodson and R. Zia, "Magnetic dipole and electric quadrupole transitions in the trivalent lanthanide series: Calculated emission rates and oscillator strengths," Phys. Rev. B **86**(12), 125102 (2012).
47. B. Rolly, B. Bebey, S. Bidault, B. Stout, and N. Bonod, "Promoting magnetic dipolar transition in trivalent lanthanide ions with lossless Mie resonances," Phys. Rev. B **85**(24), 245432 (2012).
48. R. Verre, Z. J. Yang, T. Shegai, and M. Käll, "Optical Magnetism and Plasmonic Fano Resonances in Metal-Insulator-Metal Oligomers," Nano Lett. **15**(3), 1952–1958 (2015).
49. F. Shafiei, F. Monticone, K. Q. Le, X.-X. Liu, T. Hartsfield, A. Alù, and X. Li, "A subwavelength plasmonic metamolecule exhibiting magnetic-based optical Fano resonance," Nat. Nanotechnol. **8**(2), 95–99 (2013).
50. H. Liu, D. A. Genov, D. M. Wu, Y. M. Liu, Z. W. Liu, C. Sun, S. N. Zhu, and X. Zhang, "Magnetic plasmon hybridization and optical activity at optical frequencies in metallic nanostructures," Phys. Rev. B **76**(7), 073101 (2007).
51. N. Liu, L. Fu, S. Kaiser, H. Schweizer, and H. Giessen, "Plasmonic Building Blocks for Magnetic Molecules in Three-Dimensional Optical Metamaterials," Adv. Mater. **20**(20), 3859–3865 (2008).
52. M. A. van de Haar, J. van de Groep, B. J. M. Brenny, and A. Polman, "Controlling magnetic and electric dipole modes in hollow silicon nanocylinders," Opt. Express **24**(3), 2047–2064 (2016).
53. A. García-Etxarri, R. Gómez-Medina, L. S. Froufe-Pérez, C. López, L. Chantada, F. Scheffold, J. Aizpurua, M. Nieto-Vesperinas, and J. J. Sáenz, "Strong magnetic response of submicron silicon particles in the infrared," Opt. Express **19**(6), 4815–4826 (2011).
54. Z. Ruan and S. Fan, "Superscattering of Light from Subwavelength Nanostructures," Phys. Rev. Lett. **105**(1), 013901 (2010).
55. A. Mirzaei, I. V. Shadrivov, A. E. Miroshnichenko, and Y. S. Kivshar, "Cloaking and enhanced scattering of core-shell plasmonic nanowires," Opt. Express **21**(9), 10454–10459 (2013).
56. W. Wan, W. Zheng, Y. Chen, and Z. Liu, "From Fano-like interference to superscattering with a single metallic nanodisk," Nanoscale **6**(15), 9093–9102 (2014).
57. J. D. Jackson, *Classical Electrodynamics* (Wiley, 1975).
58. E. D. Palik, *Handbook of optical constants of solids* (Academic, 1985).

1. Introduction

Dielectric nanostructures with high refractive index have recently attracted much attention as they exhibit strong optical responses while their material losses are low [1,2]. The strong optical responses can be induced by resonant magnetic modes as well as electric modes. These properties make dielectric nanostructures attractive for many applications such as metasurfaces [3–7], matematerials [8–10], solar cells [11,12], optical antannas [13–18], and nonlinear optics [19–21]. The common building blocks involved in these applications are simple dielectric nanoresonators including spherical particles [22–26], cylinders or disks [27–30], rectangular nanowires [31,32], and nanoblocks [33]. The optical properties of these individual structures have also been widely investigated. The electric and magnetic dipole resonances are two basic modes that can be readily excited in these structures. The near-field couplings between dielectric nanostructures have also drawn a lot of interest. Hybridizations of electric and magnetic modes through near-field interactions in dielectric dimer structures have been studied [34,35]. The hybridizations can induce shifts of the spectral peaks in the hybrid systems. Electric–electric, magnetic–magnetic and electric–magnetic modes couplings have been found to be involved in the hybridizations. Fano resonance, which is caused by constructive and destructive near-field interferences between different modes, has also been reported in many dielectric structures [36–40]. Fano interference usually induces a sharp dip

Optics EXPRESS

on the scattering (absorption or extinction) response spectrum (or a sharp peak on transmission spectrum) of a coupled system.

The readily excited magnetic modes (e.g., magnetic dipole mode) in dielectric nanostructures are usually accompanied by considerable magnetic field enhancement [41–43]. One straightforward application of the magnetic field enhancement is to modify the excitation and emission properties of magnetic dipole transitions [44–46] in the lanthanide ions such as Er^{3+}, Ho^{3+} and Dy^{3+} [47]. Some specifically designed plasmonic nanostructures can also support considerable magnetic field enhancement [48–51]. However, these structures are more complex. Furthermore, the high material losses in plasmonic structures lead to heating and low quantum efficiency. These disadvantages of plasmonic structures limit their applications in the field enhanced spectroscopies. Thus, high-index dielectric structures with low loss can be an attractive alternative to their plasmonic counterparts. In order to obtain strong couplings between photonic nanostructures and magnetic dipole emitters, significant magnetic field enhancement in the nanostructures is usually required. For simple dielectric structures, one important feature is that their magnetic fields are usually distributed within the entire structure volume, for example, the magnetic field of the magnetic dipole mode of a nanodisk [44,52]. Unfortunately, this kind of distribution is unfavorable to getting strong enough magnetic field enhancements. For example, dielectric dimers have been proposed to obtain electric hotspots in the gap [41,42]. However, the magnetic field enhancement in the gap of such dimers (less than 10) is even smaller than that inside the structure. Moreover, without energy concentration, how to further increase the magnetic field enhancement in the dielectric structures is not intuitive.

In this work, we show theoretically that the magnetic field enhancement in dielectric structures can be boosted by introducing radiative couplings between magnetic modes. The all-dielectric system is a concentric structure consisting of a hollow nanodisk and a ring. The hollow disk has a magnetic dipole mode. The ring has two stacked magnetic dipole modes which form a quadrupole-like mode. The resonant modes on the disk and the ring can undergo strong radiative interactions which lead to a net constructive coupling effect. As a result, a significant enhancement of the scattering cross-section with sharp peak can be obtained on the scattering spectrum for such a structure with lossless material n = 3.3. The corresponding magnetic field enhancement at the center of the disk reaches 96 times. This enhancement is about 7 times higher than that of an individual disk. The design of geometric parameters for such a system is also discussed. The structures with lossy material are also considered, where silicon (Si) is used as the material. Radiative couplings and boosted magnetic field can also be obtained. Our study reveals the strong radiative coupling of magnetic modes in dielectric structures and the corresponding boosted magnetic field enhancement effect. These results enrich our knowledge about mode couplings in dielectric structures and can find applications in field-enhanced spectroscopies, for example, the fluorescence of a magnetic dipole emitter.

2. Results and discussion

We first investigate the optical properties of individual dielectric nanostructures. The refractive index of the structures is taken to be n = 3.3 (e.g., GaP at proper wavelengths). The index of surrounding medium is taken to be 1. The optical responses are calculated by using commercial finite-difference time-domain (FDTD) software (Lumerical FDTD). Figure 1(a) shows the scattering cross-section spectrum of a hollow nanodisk. The disk is excited by a normal incident plane wave. The radius and height of the disk are 75 and 210 nm, respectively. The diameter of the hole in the center of the disk is 10 nm. Here, a small hole is introduced in the disk to make the magnetic field easily accessible to other structures [42,50], for example, the lanthanide ions. A peak appears at λ = 635 nm on the scattering spectrum. This peak corresponds to a magnetic dipole mode which can be identified by the magnetic field enhancement ($|\mathbf{H}|/|\mathbf{H}_0|$) distribution as shown in Fig. 1(a). As the size of the hole is so

Optics EXPRESS

small in comparison with that of the disk, both the mode position and $|\mathbf{H}|/|\mathbf{H}_0|$ distribution are weakly affected by the hole (data not shown). Therefore, the $|\mathbf{H}|/|\mathbf{H}_0|$ in the center of the hollow disk is similar to that of the corresponding solid disk. The $|\mathbf{H}|/|\mathbf{H}_0|$ of the magnetic dipole mode is noted to be distributed widely in the entire structure, which has been demonstrated in many other works. It can also be easily verified that the peak at λ = 518 nm corresponds to a magnetic quadrupole mode. The spectrally broad response of the electric dipole mode also contributes to the magnitude of the peaks at λ = 518 nm and 635 nm, but the electric dipole mode itself does not show a peak here. Similar results have been reported in some spheres [53].

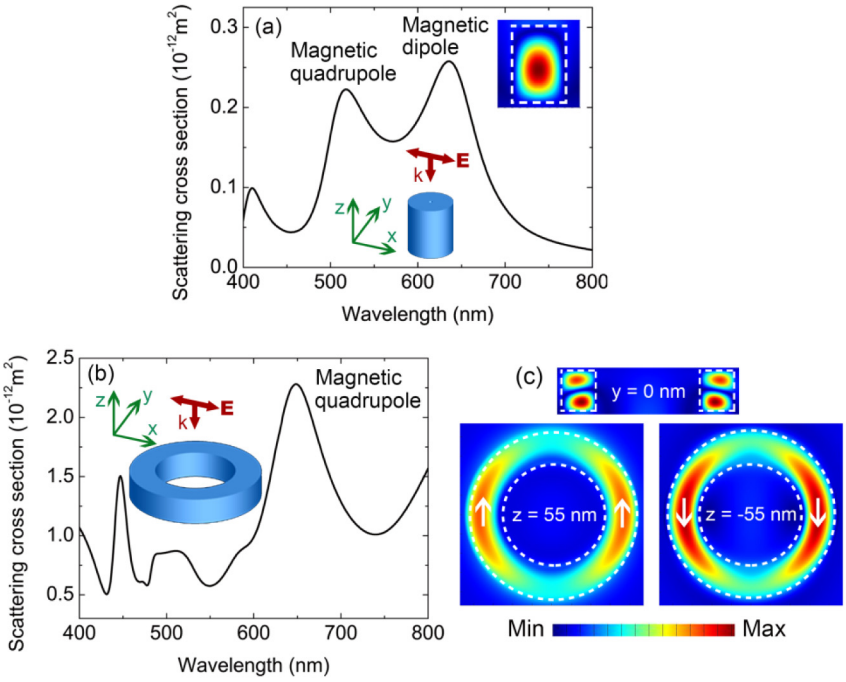

Fig. 1. Optical responses of individual disk and ring. (a) Scattering spectrum of a hollow nanodisk. The radius and height are 75 and 210 nm, respectively. The diameter of the hole is 10 nm. The refractive index is n = 3.3. The bottom inset shows the schematic of the structure with plane wave excitation. The origin of the coordinate system is placed at the center of the disk. The top inset shows the magnetic field enhancement on the y = 0 plane. The wavelength is λ = 635 nm. The dashed white line shows the edge of the disk. (b) Scattering spectrum of a ring. The inner and outer radius are R_{in} = 270 and R_{out} = 450 nm, respectively. The height is 210 nm. The refractive index is n = 3.3. The inset shows the schematic of the structure and the origin of the coordinate system is placed at the center of the ring. (c) Magnetic field enhancements of the ring on the planes of y = 0, z = 55, z = –55 nm. The wavelength is λ = 650 nm. The dashed lines represent the edge of the ring. The arrows show the directions of the magnetic field.

The height of the ring is the same as that of the disk (210 nm). The inner and outer radius of the ring are R_{in} = 270 and R_{out} = 450 nm, respectively. With the chosen geometric parameters, a resonance peak is found around λ = 650 nm (Fig. 1(b)). This resonance position is close to that of the magnetic dipole mode on the disk. The magnetic near field distributions are also calculated in order to identify the mode here (Fig. 1(c)). The magnetic field distribution of this mode can be divided into the top and bottom regions inside the ring. The arrows in Fig. 1(c) denote the main feature of the calculated magnetic field directions (this can be easily verified by the calculated magnetic field vector distributions). The magnetic field enhancement in the ring is dominated by the y-axis component ($|\mathbf{H}_y|/|\mathbf{H}_0|$).The magnetic

Optics EXPRESS

fields in the top and bottom regions are out of phase. The field in each region (the top or bottom one) can be taken as a magnetic dipole mode. So the combination of the fields in the two regions gives a magnetic quadrupole-like mode. In fact, this mode can be equivalently taken as a magnetic quadrupole mode on an infinite rod with TM excitation (this will be discussed later), where the cross-section size of the infinite rod is the same as that of the ring rod.

Now let us turn to the coupled system as shown in Fig. 2(a). The coupled system consists of the disk and ring discussed above. The index of surrounding medium is also 1. The origin of the coordinate system is chosen at the center of the disk (Fig. 2(a)). The structure is excited by a plane wave with normal incidence. The scattering spectrum of the coupled system is shown in Fig. 2(b). A sharp peak at λ = 635 nm is seen on the spectrum. The peak position is close to the resonance positions of the individual disk and ring. This spectral phenomenon is similar to that of the superscattering discussed in plasmonic subwavelength nanostructures [54–56]. But the mechanism in this system is different from that in the superscattering phenomenon. The superscattering in plasmonic nanostructures is caused by the near field couplings of different electromagnetic modes. Here, the enhanced scattering is caused by radiative couplings of magnetic modes.

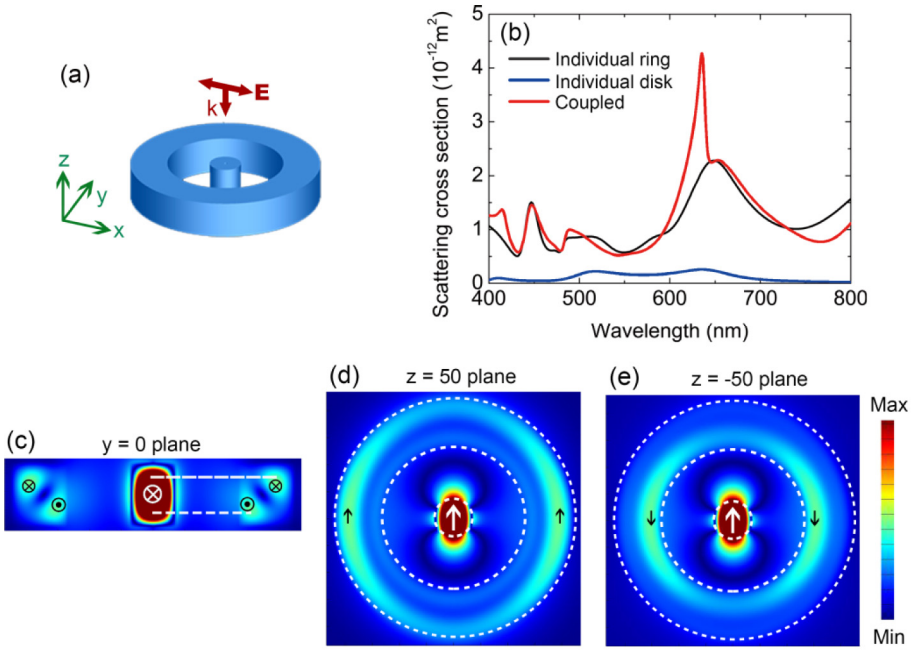

Fig. 2. Superscattering-like spectral phenomenon induced by radiative couplings of the magnetic modes on the disk and ring. (a) Schematic of the coupled system. The structure is excited by a plane wave with normal incidence plane wave. The origin of coordinate system is placed at the center of the disk. (b) Scattering spectrum of the coupled system. The geometries of the ring and disk are the same as that in Fig. 1. The scattering spectra of the individual disk and ring are also shown for comparison. (c-e) Magnetic field enhancements of the ring on the planes of y = 0, z = 50 and z = –50 nm. The wavelength is λ = 635 nm. The arrows denote the directions of the magnetic field.

In order to understand the coupling of magnetic modes in our system, the magnetic field distributions at the sharp peak (λ = 635 nm) are calculated. The magnetic field distributions on the planes of y = 0, z = 50 and z = –50 nm are shown in Figs. 2(c), 2(d) and 2(e), respectively. The effects of near-field couplings can be ignored here as the distance between the modes of the disk and the ring is so large (>200 nm). The magnetic field of the coupled

Optics EXPRESS

ring is rotated (Fig. 2(c)) in comparison with the case of the individual ring (Fig. 1(c)), which leads to an inner and an outer magnetic dipole mode. The two magnetic dipole modes of the ring can both interact radiatively with the magnetic dipole mode of the disk. The magnetic dipole-dipole interaction potential energy H with spatial phase retardation can be expressed as [57]

$$H = -\frac{\mu_0}{4\pi|\mathbf{r}|^3}(3(\mathbf{m}_1\cdot\hat{\mathbf{r}})(\mathbf{m}_2\cdot\hat{\mathbf{r}})-\mathbf{m}_1\cdot\mathbf{m}_2)e^{i\omega|\mathbf{r}|/c}, \quad (1)$$

where $\mathbf{m}_1$ and $\mathbf{m}_2$ are the interacting magnetic dipole moments, μ_0 is the magnetic constant, $\hat{\mathbf{r}}$ is a unit vector parallel to the line joining the centers of the two dipoles, $|\mathbf{r}|$ is the distance between the centers of $\mathbf{m}_1$ and $\mathbf{m}_2$, ω and c are the angular frequency and speed of light, respectively. A positive (negative) H means a constructive (destructive) coupling between the two magnetic dipoles. Let us first investigate the magnetic mode couplings on the representative plane of $y = 0$. The magnetic fields of the disk and the ring on this plane are both only in the y-axis direction, and their directions are shown in Fig. 2(c). The interaction energy H of the inner (outer) dipole mode on the ring and the dipole mode on the disk is denoted by $H_{\text{in}}^{y=0}$ ($H_{\text{out}}^{y=0}$). For simplicity, the magnetic dipole moments of the inner and outer modes of the ring are approximately taken as the same value. Then we have $H_{\text{in}}^{y=0} \propto -\frac{e^{i\omega|\mathbf{r}_{\text{in}}|/c}}{|\mathbf{r}_{\text{in}}|^3}$ ($H_{\text{out}}^{y=0} \propto -\frac{e^{i\omega|\mathbf{r}_{\text{out}}|/c}}{|\mathbf{r}_{\text{out}}|^3}$), where $|\mathbf{r}_{\text{in}}|$ ($|\mathbf{r}_{\text{out}}|$) is the distance between the inner (outer) magnetic dipole mode of the ring and the magnetic dipole mode of the disk. $|\mathbf{r}_{\text{in}}|$ and $|\mathbf{r}_{\text{out}}|$ determine the sign and relative magnitude of the H value. In our case, the $|\mathbf{r}_{\text{in}}|$ and $|\mathbf{r}_{\text{out}}|$ are approximately taken as 300 nm and 400 nm, respectively (white dashed lines in Fig. 2(c)). One obtains a positive $H_{\text{in}}^{y=0}$ and a negative $H_{\text{out}}^{y=0}$, but the magnitude of $H_{\text{in}}^{y=0}$ is about 3.4 times higher than that of the $H_{\text{out}}^{y=0}$. So we get a net constructive coupling between the magnetic modes of the ring and the disk.

On the other planes (e.g., the $y = 0$ plane rotated around the z-axis), there are also magnetic field distributions on the structure. For the disk, the magnetic field enhancement is still dominated by the y-axis component, the magnetic field enhancements in the x-axis and z-axis directions can be ignored. For the ring, the magnetic field enhancement in the x-axis direction can be ignored (data not shown). There is certain magnetic field enhancement in the z-axis direction. But the magnetic dipole in z-direction on the ring does not radiatively interact with the magnetic dipole mode on the disk. This is due to the fact that the magnetic dipole moment in z-axis direction on the ring is perpendicular to both the dipole moment of the disk and the $\hat{\mathbf{r}}$. Therefore, only the magnetic field in the y-axis direction needs to be considered here. The corresponding magnetic field enhancements in the y-axis direction are shown in Figs. 2(d) and 2(e). The magnetic field on the ring is mainly distributed around the $y = 0$ plane. Thus, the radiative interactions between the modes on the other planes of the coupled structure also result in a net constructive coupling effect.

One significant effect of the net constructive radiative coupling is the enhanced optical responses of the disk. Figure 3 shows the magnetic and electric near field enhancements of the coupled system. The $|\mathbf{H}|/|\mathbf{H}_0|$ at the center of the disk reaches a value around 96 at the peak. This enhancement is about 7 times higher than that of the individual disk (Fig. 3(a)). The $|\mathbf{H}|/|\mathbf{H}_0|$ distribution profile of the disk in the coupled system keeps nearly the same as that of the individual disk (Figs. 3(b) and 1(a)). Considerable value of the electric near field enhancement $|\mathbf{E}|/|\mathbf{E}_0|$ of the coupled disk is also seen (Fig. 3(c)). There is almost no electric field enhancement at the center of the disk, which gives us a pure magnetic near-field hot spot

Optics EXPRESS

at the center of the disk. This feature is important for the excitation of magnetic dipole transitions [45]. Here it should be pointed out that the surrounding medium has been assumed to be 1. We have also calculated the cases with structures on substrates (data not shown). The $|\mathbf{H}|/|\mathbf{H}_0|$ of coupled disk/ring structure decreases with substrates. For example, the $|\mathbf{H}|/|\mathbf{H}_0|$ for a coupled structure placed on a substrate with refractive index n = 1.4 reduces to about 48 which is half of that in vacuum. But since the $|\mathbf{H}|/|\mathbf{H}_0|$ of an individual disk on substrate also reduces, the enhancement of 48 is still about 4.5 times higher than that of the individual disk on the substrate. It is also noted that the coupling involves the quadrupole-like mode of the ring, where the magnetic fields in the top and bottom regions are out of phase. The excitation efficiency of this mode is sensitive to the angle of incidence. Thus, the coupled system with oblique incidence gives a reduced $|\mathbf{H}|/|\mathbf{H}_0|$. For example, the incidence with an angle of 30° gives the $|\mathbf{H}|/|\mathbf{H}_0|$ of ~50 which is smaller than that with the normal incidence.

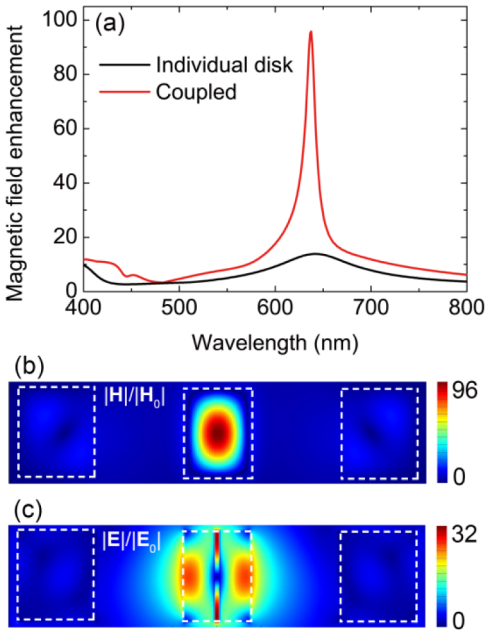

Fig. 3. Boosted magnetic field enhancement. (a) Magnetic field enhancement at the center of the hollow disk in the coupled structure (red). The case for an individual disk (black) is also shown for comparison. (b,c) The magnetic and electric field enhancements of the coupled structure on the plane of $y = 0$ plane. The wavelength is λ = 635 nm. The dashed lines show the outline of the structures.

For a given disk with a magnetic dipole resonance, a dielectric ring with the magnetic quadrupole-like mode has been demonstrated to be able to cause the superscattering-like spectral phenomenon and the boosted magnetic field enhancement in the coupled system. However, there are usually many different modes on the rings with different inner or outer radii. These modes make the design of a ring for the resonant quadrupole-like mode complex and time consuming. Now let us discuss how to efficiently design the geometric parameters of a ring to achieve the boosted magnetic field enhancement. For this purpose, we first study the effects of the geometric parameters of the ring on the $|\mathbf{H}|/|\mathbf{H}_0|$ of the disk (Figs. 4(a)-4(c)). Figure 4(a) shows the $|\mathbf{H}|/|\mathbf{H}_0|$ spectra with different R_{out} of the ring, where the R_{in} is fixed at R_{in} = 270 nm. For each R_{out}, there is a peak value on the $|\mathbf{H}|/|\mathbf{H}_0|$ spectrum. The peak of $|\mathbf{H}|/|\mathbf{H}_0|$ reaches maximal value at R_{out} = 450 nm. This is reasonable as the quadrupole-like mode of a ring with this geometric size is spectrally close to the magnetic dipole mode of the disk (Figs. 1 and 2). Similar calculations have also been carried out for cases with other R_{in} such as R_{in} = 215 (Fig. 4(b)) and 300 nm (Fig. 4(c)). For each of these R_{in}, the peak of the

Optics EXPRESS

$|\mathbf{H}|/|\mathbf{H}_0|$ always reaches the maximal value with the same rod width of the ring (R_{out} - R_{in} = 180 nm). More calculations show that the resonance positions of these individual rings, which have different R_{in} but the same R_{out} - R_{in} = 180 nm, are all close to that of an infinite rod with the width 180 nm (Fig. 4(d), the thickness of the rings and the rod is always fixed at the same value 210 nm). Here, the infinite rod is excited by a TM polarized plane wave. The resonant magnetic field profile of the infinite rod also reproduces those of the individual rings (Figs. 4(b) and 1(c)). So the quadrupole-like mode on a ring can be equivalently taken as a special formation of the magnetic quadrupole mode on the corresponding infinite rod, where the geometric parameters (the width and height) of the ring are the same as that of the infinite rod. This equivalence is useful in practical calculations as the simulations for the quadrupole mode on infinite rods (simulations are done in two-dimensional) are much easier and faster than those for the quadrupole-like mode in rings (simulations are done in three-dimensional).

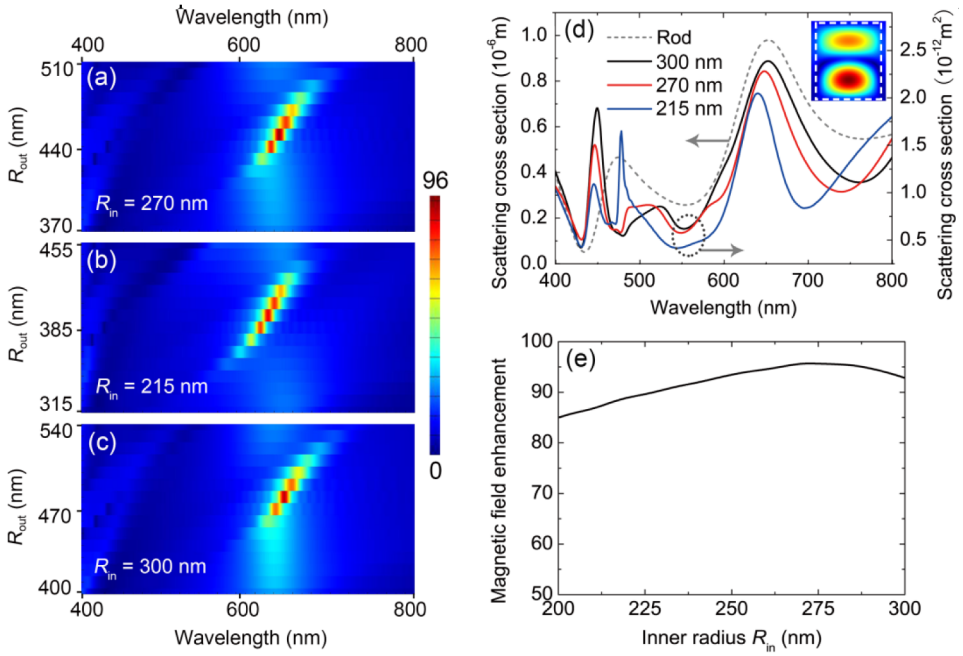

Fig. 4. Designing the coupled system to boost the magnetic field enhancement. (a-c) The magnetic field enhancement at the center of the disk in coupled structure as a function of wavelength and R_{out} with R_{in} = 270, 215 and 300 nm. (d) Scattering spectrum of individual rings with R_{in} = 300 (black), 270 (red) and 215 nm (blue). The corresponding R_{out} are R_{out} = 480, 450 and 395 nm, respectively. The case for an individual infinite rod with width 180 nm and height 210 nm is also shown (dashed gray). The inset shows the magnetic field distribution of the infinite rod at λ = 650 nm. (e) The peak magnetic field enhancement at the center of the disk as function of inner radius R_{in} of a ring. The R_{out} - R_{in} is fixed at 180 nm for all the rings.

The geometric size of the ring is also an important factor that affects the $|\mathbf{H}|/|\mathbf{H}_0|$ value around the disk. As discussed above, to obtain the maximal $|\mathbf{H}|/|\mathbf{H}_0|$ for a given R_{in}, the R_{out} should be chosen that the quadrupole-like mode on the ring is spectrally close to the magnetic dipole mode on the disk, which results in the same rod width (R_{out} - R_{in}) for rings with different R_{in}. In our case, the R_{out} - R_{in} is 180 nm. So one can exact the peak $|\mathbf{H}|/|\mathbf{H}_0|$ value at the center of the disk as a function of R_{in} as shown in Fig. 4(e). An optimized peak $|\mathbf{H}|/|\mathbf{H}_0|$ is seen around R_{in} = 270 nm. At other R_{in} (between 200 and 300 nm in our study), the peak $|\mathbf{H}|/|\mathbf{H}_0|$ becomes smaller but still keeps relatively high value. The variation of the peak $|\mathbf{H}|/|\mathbf{H}_0|$ with different R_{in} (Fig. 4(e)) can be explained by combining the effects of the magnetic dipole coupling strength and phase differences in the radiative interactions (Eq. (1)). For a smaller R_{in}, the coupling strength is larger (smaller dipole-dipole distance) but the phase

Optics EXPRESS

factor contribution ($e^{i\omega|\mathbf{r}|/c}$) is smaller. The situation is reversed for a larger R_{in}. So the combination of these two factors results in the optimized $|\mathbf{H}|/|\mathbf{H}_0|$ at a proper ring size (R_{in} = 270 nm). This R_{in} will make the $|\mathbf{r}_{in}|$ (~300 nm, Fig. 2) close to half of the working wavelength ($\lambda/2 \approx 317$ nm) and thus $\omega|\mathbf{r}_{in}|/c$ close to π, which leads to strong constructive coupling between the inner magnetic mode of the ring and the magnetic mode of the disk. It should be pointed out that the results in Fig. 4(e) indicate again that the coupling between the disk and the ring is not a near-field interaction. Let us focus on the results with R_{in} = 215 nm and 270 nm. It can be easily verified that the near field enhancement of the ring with R_{in} = 215 nm is slightly larger than that with R_{in} = 270 nm (data not shown). If the coupling was a near-field interaction, the $|\mathbf{H}|/|\mathbf{H}_0|$ of the disk with R_{in} = 215 nm should be larger as the gap between the disk and ring is smaller. But our direct calculations give the opposite results.

Based on the discussion about Fig. 4, the coupling system can be designed in the way that for a given disk the R_{in} of the ring is a little smaller than half of the resonance wavelength and the R_{out} should be chosen that the quadrupole mode of the equivalent infinite rod is spectrally close to the dipole mode of the disk. For example, we have tried the case of a smaller disk (n = 3.3) with resonance at λ = 450 nm. The size of ring can be easily obtained in this way to make the system undergo strong constructive radiative coupling and the boosted magnetic field enhancement (~90). In fact, as the refractive index is also n = 3.3 and the modes are leaky geometrical resonances, the system with resonance at λ = 450 nm can also be obtained by directly shrink the size of the system. The system now has a height of 150 nm. Thus, for a given material, increasing the height will cause the resonant system to be enlarged and the redshift of the resonance peak. However, the field enhancement value does not show obvious change with height (the enhancements are 90 and 96 for the heights of 150 and 210 nm, respectively).

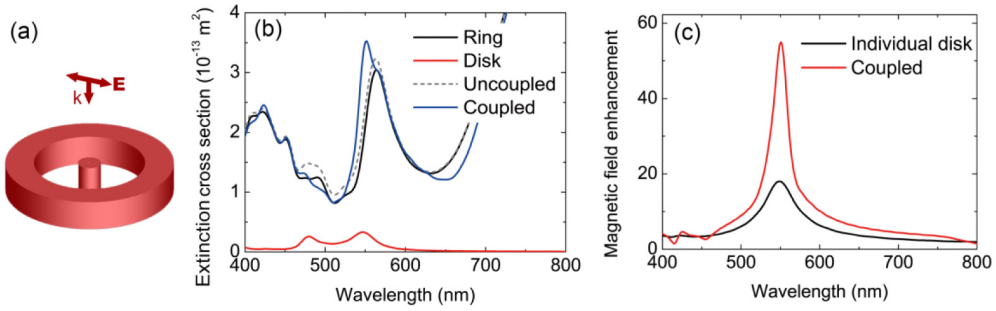

Fig. 5. Boosting magnetic field enhancement in a lossy system with Si as the material. (a) The schematic of the coupled system consisting of a disk and a ring. (b) Extinction spectra of the coupled system and individual disk and ring. The radius and height of the disk are 52.5 and 150 nm, respectively. The diameter of the hole in the disk is also 10 nm. The inner and outer radius of the ring are R_{in} = 250 and R_{out} = 380 nm, respectively. The height of the ring is 150 nm. (c) The magnetic field enhancement at the center of the disk in the coupled structure (red) and the individual disk (black).

We have focused on the systems without loss, now let us turn to the dielectric structures with lossy material (Fig. 5(a)). We choose the widely investigated Si as the material and the dielectric constants are taken from Palik's book [58]. The design of this system follows the way that has been discussed in Fig. 4. We first choose a working wavelength at λ = 550 nm. A disk with radius 52.5 nm, height 150 nm and hole diameter 10 nm satisfies that the magnetic dipole mode is around λ = 550 nm. The R_{in} of the ring is chosen to be R_{in} = 250 nm and the R_{out} is calculated to be R_{out} = 380 nm to make the quadrupole-like mode of the ring spectrally close to the magnetic dipole mode on the disk. As material loss is introduced in this system, extinction cross-section instead of scattering cross-section is now used to demonstrate the far field responses (Fig. 5(b)). Enhanced extinction cross-section phenomenon is obtained, which

Optics EXPRESS

indicates that the constructive radiative magnetic mode couplings occur in this system. This spectral phenomenon is similar to the lossless structure discussed in Fig. 2. Calculations show that the absorption of the disk is significantly enhanced by the radiative couplings. The $|\mathbf{H}|/|\mathbf{H}_0|$ in the center of the disk reaches 55 at the peak and this enhancement is 3 times higher than that of the individual disk (Fig. 5(c)).

3. Conclusion

In conclusion, we have shown that significant radiative couplings between magnetic modes can be obtained in all-dielectric nanostructures and this phenomenon can be used to boost the magnetic field enhancement. The coupling involves magnetic dipole mode on a disk and two magnetic dipole modes on a ring. In the investigated case with $n = 3.3$ (e.g., GaP), the $|\mathbf{H}|/|\mathbf{H}_0|$ at the center of the disk reaches 96 which is about 7 times higher than that of the individual disk. The effect of the geometries of the ring on the $|\mathbf{H}|/|\mathbf{H}_0|$ has also been studied and the results give us effective guidance on how to design this kind of system. We have also shown that the radiative coupling of magnetic modes and the corresponding boosted magnetic field enhancement can be obtained in a lossy dielectric system where Si is used as the material. For a case with working wavelength $\lambda = 550$ nm, the $|\mathbf{H}|/|\mathbf{H}_0|$ can reach 55 which is about 3 times higher than that of the individual Si disk. Although the interactions involve radiative couplings here, the sizes of the structures are around wavelength scale (smaller than 1.5λ) and the size of the boosted magnetic field is in deeply subwavelength scale. The strong magnetic field enhancement in such structures can be used to tailor the optical properties of magnetic dipole emitters, and the strong radiative coupling of magnetic modes could also find applications in other photonic devices.

Funding

Hunan Provincial Natural Science Foundation of China (Grant no. 2017JJ3408); National Natural Science Foundation of China (NSFC) (Grant no. 61222406, 11174371).